HHS Public Access

Author manuscript

ACS Appl Mater Interfaces. Author manuscript; available in PMC 2017 July 20.

Published in final edited form as:

ACS Appl Mater Interfaces. 2016 July 20; 8(28): 17955–17963. doi:10.1021/acsami.6b05840.

Accelerated Blood Clearance Phenomenon Reduces the Passive Targeting of PEGylated Nanoparticles in Peripheral Arterial Disease

Hyung-Jun Im[1,2,‡], **Christopher G. England**[3,‡], **Liangzhu Feng**[4], **Stephen A. Graves**[3], **Reinier Hernandez**[3], **Robert J. Nickles**[3], **Zhuang Liu**[4], **Dong Soo Lee**[2], **Steve Y. Cho**[1], and **Weibo Cai**[1,3,5,*]

[1]Department of Radiology, University of Wisconsin - Madison, WI 53705, USA

[2]Department of Molecular Medicine and Biopharmaceutical Sciences, Department of Nuclear Medicine, Seoul National University, Seoul 110-744, Korea

[3]Department of Medical Physics, University of Wisconsin - Madison, Madison, WI 53705, USA

[4]Jiangsu Key Laboratory for Carbon-Based Functional Materials & Devices Laboratory, Soochow University Suzhou, Jiangsu 215123, China

[5]University of Wisconsin Carbone Cancer Center, Madison, WI 53705, USA

Abstract

Peripheral arterial disease (PAD) is a leading global health concern. Due to limited imaging and therapeutic options, PAD and other ischemia-related diseases may benefit from the use of long circulating nanoparticles as imaging probes and/or drug delivery vehicles. Polyethylene glycol (PEG)-conjugated nanoparticles have shown shortened circulation half-lives *in vivo* when injected multiple times into a single subject. This phenomenon has become known as the accelerated blood clearance (ABC) effect. The phenomenon is of concern for clinical translation of nanomaterials as it limits the passive accumulation of nanoparticles in many diseases, yet it has not been evaluated using inorganic or organic-inorganic hybrid nanoparticles. Herein, we found that the ABC phenomenon was induced by re-injection of PEGylated long circulating organic-inorganic hybrid nanoparticles, which significantly reduced the passive targeting of ^{64}Cu-labeled PEGylated reduced graphene oxide – iron oxide nanoparticles (^{64}Cu-RGO-IONP-PEG) in a murine model of PAD. Positron emission tomography (PET) imaging was performed at 3, 10, and 17 days post-surgical induction of hindlimb ischemia. At Day 3 post-surgery, the nanoparticles displayed a long circulation half-life with enhanced accumulation in the ischemic hindlimb. At Day 10 and 17 post-surgery, re-injected mice displayed a short circulation half-life and lower accumulation of the

*Corresponding Author: Weibo Cai, Ph.D., Departments of Radiology and Medical Physics, University of Wisconsin - Madison, Room 7137, 1111 Highland Ave, Madison, WI 53705-2275, USA. wcai@uwhealth.org; Phone: 608-262-1749; Fax: 608- 265-0614.
‡These authors contributed equally to this work

Supporting Information. Characterization of the nanomaterials and quantitative uptake determined by positron emission tomography (PET) imaging

Author Contributions: The manuscript was written through contributions of all authors. All authors have given approval to the final version of the manuscript.

Disclosure Statement: The authors declare that they have no competing financial interests.

nanoparticles in the ischemic hindlimb, in comparison to the naïve group. Also, re-injected mice showed significantly higher liver uptake than the naïve group, indicating that the nanoparticles experienced higher sequestration by the liver in the re-injected group. Furthermore, photoacoustic (PA) imaging and Prussian blue staining confirmed the enhanced accumulation of the nanoparticles in the liver tissue of re-injected mice. These findings validate the ABC phenomenon using long circulating organic-inorganic hybrid nanoparticles upon multiple administrations to the same animal, which may provide valuable insight into the future clinical applications of nanoparticles for imaging and treatment of PAD.

Graphical abstract

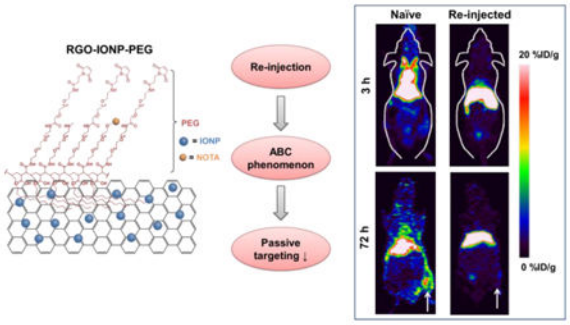

Keywords

Accelerated blood clearance (ABC); peripheral arterial disease; reduced graphene oxide (RGO); iron oxide nanoparticle (IONP); anti-PEG antibody; hindlimb ischemia; positron emission tomography (PET); photoacoustic imaging

Introduction

Peripheral arterial disease (PAD) results from the atherosclerotic stenosis of the peripheral arteries, especially in the lower extremities, and has become one of the major health concerns in elderly patients as it affects more than 200 million worldwide.[1-2] The restricted supply of oxygenated blood to the peripheral tissues results in intermittent claudication, slower wound healing, and possible gangrene in severe cases.[3] Critical limb ischemia (CLI) is the most severe form of PAD and is the leading cause of limb amputation worldwide.[4] Current treatment options for CLI include peripheral artery bypass surgery, proangiogenic growth factor therapy, and anti-platelet medications.[5] While surgical intervention is most effective, bypass surgery has been linked to several adverse effects, including heart attack, stroke and infection. It has been shown that revascularization surgery works for only ~40% of patients with CLI, which is why many patients rely upon other treatment options.[6] Proangiogenic growth factor (PGF) therapy has been proposed to enhance the microvascular circulation,[7-8] yet low delivery efficiency and systemic off-target toxicites have effectively hampered the benefits of PGF treatment.[5] Additionally, some non-aspirin antiplatelet therapies (e.g., clopidogrel and ticlopidine) have reduced cardiovascular events in patients with PAD; yet these drugs fail to elicit symptomatic improvement in patients with intermittent claudication.[5, 9] For these reasons, nanoparticle-based proangiogenic gene or

growth factor delivery provides an alternative method to overcome the limitations of traditional treatment modalities. In particular, preclinical investigation of nanoparticle-based growth factor treatment showed significant improvement of the perfusion in a PAD model.[10]

We recently developed a long circulating organic-inorganic hybrid nanoparticle by coating two layers of polyethylene glycol (PEG) onto reduced graphene oxide iron oxide nanoparticles (RGO-IONP-PEG). RGO-IONP-PEG displays excellent theranostic properties which may be suitable for PAD imaging and therapy. The low perfusion rate found in PAD requires that successful imaging or therapeutic agents display long blood circulation times with high passive targeting capabilities. Previously, RGO-IONP-PEG was shown to display a long circulation half-life and excellent passive targeting efficiency in a tumor model of mouse.[11] In addition, RGO-IONP-PEG can load and deliver large drug payloads to diseased tissues, further proving that this nanoparticle may be a prime candidate for imaging-guided drug delivery in PAD.[12]

Accelerated blood clearance (ABC) phenomenon refers to the significantly decreased circulation half-life displayed by PEGylated nanomaterials when repeatedly injected *in vivo*.[13] The phenomenon was initially observed with PEGylated liposome,[14] yet has been reproduced using several nanoplatforms, including micelles[15] and PLGA nanoparticles.[16] This phenomenon is thought to be a result of increased splenic production of anti-PEG IgM.[17-18] While it has been investigated with lipid or polymer based nanoparticles, there are no reports evaluating the ABC phenomenon using inorganic or organic-inorganic hybrid nanoparticles.

In this work, we hypothesized that re-injection of PEGylated RGO-IONP will induce the ABC phenomenon, resulting in a significant decrease in the circulation half-life and passive targeting capabilities of these nanoparticles. By comparing the re-injected group with mice that were not re-injected (naïve), we verified that the circulation half-life and passive accumulation of RGO-IONP-PEG in the ischemic tissues was significantly decreased. A murine model of PAD was produced by ligation and cut of the femoral artery. At 3, 10, and 17 days post-surgery, mice were scanned for up to 72 h with PET after receiving an intravenous injection of ^{64}Cu-RGO-IONP-PEG. As the ischemic hindlimb heals post-surgery, vasculature normalization will result in decreased nanoparticle accumulation as the enhanced permeability and retention (EPR) effect is diminished.[19] Two different animal groups were utilized, including a naïve group in which different mice were used at each time point (Day 3, 10, and 17 post-surgery) and a re-injected group with mice that were serially injected at Days 3, 10, 17 post-surgery. At Day 10 and 17 post-surgery, the re-injected group showed faster blood clearance and higher liver uptake of the nanoparticle, as compared to the naïve group, validating the effects of the ABC phenomenon. Also, decreased nanoparticle accumulation in the ischemic hindlimb of re-injected mice indicated that passive targeting was effectively reduced by ABC effect. The phenomenon was considered to be mediated by anti-PEG IgM, based on ELISA results showed that Anti-PEG IgM was present at 7 and 14 days after injection of the nanoparticles. Furthermore, we confirmed that the nanoparticles were cleared to the liver, using photoacoustic image, and histologic examination of liver tissue.

Experimental Section

RGO-IONP-PEG Production and PEGylation

The syntheses of nanoparticles (RGO-IONP-PEG) were previously provided. [20] Synthesis of the nanoparticles was accomplished using a modified version of the Hammer method. As PEGylation improves the overall circulation of nanoparticles, 10 mg of poly(maleicanhydride-alt-1-octadecene) (PEG) (Sigma-Aldrich, Madison, WI, USA) was used to functionalize RGO-IONP (1 mg). An additional layer of PEG was conjugated to increase circulation time. Also NOTA was conjugated for radiolabeling. p-SCN-Bn-NOTA (NOTA, Macrocyclics, Inc., Dallas, TX, USA) was conjugated to the nanoparticles with 1:4 molar ratio of nanoparticle: chelator. NOTA was conjugated to the nanoparticles post-PEGylation. NOTA-RGO-IONP characterization was reported in previous work.[11]

Murine Model of Hindlimb Ischemia

All animal studies were conducted under a protocol approved by the University of Wisconsin Institutional Animal Care and Use Committee. Using six-week-old female BALB/c mice (Harlan, Indianapolis, IN), right unilateral hindlimb ischemia was produced as previously described.[21] Briefly, an incision at the mid-abdominal level was made to expose the femoral triangle, after the mice were anesthetized with 2% isoflurane. Using an intraoperative microscope, the right femoral artery was isolated from the femoral vein and nerve, and the artery was sutured in two locations and cut in-between to disrupt the blood flow using nylon sutures (6/0; ARO Surgical Corp., Newport Beach, CA).

Laser Doppler Perfusion Imaging

Imaging of both hindlimbs were performed before and directly after surgical induction of ischemia using the high resolution moorLDI2-HR laser Doppler imager (Moor Instruments, DE, USA).

Radiolabeling of RGO-IONP-PEG

^{64}Cu production was previously described.[22] Briefly, $^{64}CuCl_2$ was mixed with 200 μL of RGO-IONP-PEG and incubated for 30 min (37 °C; 550 rpm). A PD-10 column was used to purify the sample from non-labeled isotope.

Positron Emission Tomography Imaging and Quantitative Analyses

The Inveon microPET/microCT rodent scanner (Siemens Medical Solutions USA, Inc.) was used for imaging after mice were injected with 8-10 MBq of radiolabeled nanoparticle. PET image acquisition, reconstruction, decay correction, and region-of-interest (ROI) analysis were carried out as previously described.[23] Quantitative PET data were presented as a percent of injected dose per gram of tissue (%ID/g) with 3-4 mice per group.

Ex Vivo Biodistribution

Biodistribution of the tracer was used to confirm results from PET imaging. After mice were euthanized, we collected the blood, major organs/tissues and ischemic/non-ischemic muscle.

Gamma radiation in the samples was measured in a Wizard 2 Automatic Gamma Counter from PerkinElmer and the values were recorded in %ID/g with 3-4 mice per group.

Histological Staining of Tissues

Histological sectioning and hematoxylin & eosin (H&E) staining of tissues was performed by the Experimental Pathology core facility at the Carbone Cancer Center. Tissues were sliced at 5-7μm and the Iron Staining Kit from Sigma-Aldrich (St. Louis, MO, USA) was used to stain iron in the tissue sections. Tissue sections were incubated in cold CH_3OH for 10-15 min before incubation with a solution of 1 part $K_4[Fe(CN)_6] \cdot 3\ H_2O$ and 1 part HCl was applied to the slides for 8-10 min before washing with cold tap H_2O. After the slides were dried and coverslipped, the slides were imaged using bright-field microscopy.

Ultrasound and Photoacoustic Imaging Techniques

Ultrasonography and photoacoustic imaging was accomplished using the Vevo LAZR System from VisualSonics (Toronto, Canada). Photoacoustic imaging was performed in the liver before and 12 h after injection of ^{64}Cu-RGO-IONP-PEG using an 808-nm laser with a depth penetration focal point of 10 mm.

Anti-PEG IgM enzyme-linked immunosorbent assay (ELISA)

Anti-PEG IgM was detected using mouse an anti-PEG IgM ELISA kit (Life diagnostics, West Chester, PA, USA). Mouse serum was collected before injection of nanoparticles and at Day 7 and 14 post-injection of ^{64}Cu-RGO-IONP-PEG (56.1 μg per mouse). Mouse serum was diluted 25-fold and dispensed into the wells. After incubation for 1 h at 100-150 rpm at room temperature, well contents were aspirated and the wells were washed five-times with 1X wash solution. Next, 100 ml of diluted horseradish peroxidase conjugate was added into each well. The wells were incubated for 30 min at room temperature with shaking at 100-150 rpm before washing five times. The 3,3′,5,5′-tetramethylbenzidine (TMB) reagent was added into each well and incubated at room temperature for 20 min. Finally, 100 ml of Stop Solution (1N HCl) was added to stop the reaction. The optical density was measured at 450 nm with a microtiter plate reader (BioTek, Winooski, VT, USA).

Statistical Tests

All values were presented as mean ± standard deviation. Student *t*-test was performed to assess the difference between the mean values from two groups, and a p value less than 0.05 was used to define statistical significance.

Results and Discussion

Synthesis of RGO-IONP-PEG

RGO-IONP-PEG was synthesized according to the procedures previously described.[20] Two layers of PEG were added to the surface of the nanoparticles to extend their circulation time. A well-known chelator for ^{64}Cu labeling, known as NOTA (1,4,7-triazacyclononane-triacetic acid), was conjugated for *in vivo* PET imaging (Figure 1a). The nanoparticles were characterized to determine the morphology, diameter and surface charge (Figure S1). The

morphology and size of the nanoparticles were examined by atomic force microscopy (AFM) and dynamic light scattering (DLS), respectively. The hydrodynamic diameter of the nanoplatform was found to be 92.68 ± 33.3 nm with a polydispersity index (PDI) of 0.16. Also, the UV-Visible spectrum was consistent with previous data, further verifying the identity of the nanoparticles.[20] In addition, the zeta potential was calculated as -10.2 ± 0.9 mV. Previously, we have shown that RGO-IONPs displays high serum stability with over 90% of radiolabeled nanoparticles remaining stable at 40 h.[11]

RGO-IONP-PEG displays excellent theranostic properties, making it suitable for both molecular imaging and therapy of many diseases, including PAD. The long circulation half-life and high passive targeting capabilities of RGO-IONP-PEG are essential for ischemic-related diseases, as the low perfusion rate can effectively limit the access of nanoparticles to the ischemic tissues. In addition to its excellent theranostic properties, ^{64}Cu-RGO-IONP-PEG can function as a triple modality imaging probe for PET, MR, and photoacoustic imaging, with each imaging modality providing essential information regarding PAD progression and therapeutic response. While PET provides high sensitivity and quantifiability needed for grading the disease severity, the high spatial resolution of MR can compensate for the low resolution of PET, making it possible to better determine the spatiotemporal localization of the disease.[20] While image-guided procedures are difficult using PET and MRI, photoacoustic (PA) imaging provides new avenues for potential image-guided therapies. Lastly, previous studies have shown that RGO-IONP-PEG can effectively load considerable drug payloads for delivery to numerous diseases.[24]

Production of Murine Model of Hindlimb Ischemia

Hindlimb ischemia was induced by ligation and cutting of the femoral artery in mice.[25] A mid-abdominal incision was made after induction of anesthesia using isoflurane (Figure 1b). After dissection of adjacent fat tissue and fascia, the femoral artery, vein and nerve were visualized. The femoral artery was isolated and ligated after separation from the femoral vein and nerve. Lastly, the femoral artery was cut to induce ischemia in the hindlimb. Laser Doppler images showed significantly decreased blood flow in the surgical hindlimb, which confirmed the successful creation of the ischemic model (Figure 1b). After surgical-induction of ischemia, the hindlimb gradually heals over time with vasculature normalizing between 20 to 30 days post-surgery.[21] As the hindlimb heals and the vascularization normalizes, the EPR effect will decrease resulting in less nanoparticle accumulation at later times post-surgery.[19] While the EPR effect has been extensively documented in cancer, activation and mobilization of endothelial cells in ischemic tissues also results in leaky vasculature, which is a key attributor to the EPR effect in solid tumors.[26]

PET Imaging and Analysis

At 3, 10 and 17 days post-surgical induction of hindlimb ischemia, mice were injected (naïve) or re-injected with ^{64}Cu-RGO-IONP-PEG and PET imaging was performed at different time points up to 72 h post-injection. At Day 3, all mice received an injection of ^{64}Cu-RGO-IONP-PEG for the first time. At Day 10 and Day 17, non-injected mice were used for naïve group, while the same mice were used for re-injected group previously injected on Day 3 post-surgery. At Day 3 post-surgery, PET imaging revealed high blood

pool uptake through 48 h post-injection. The nanoparticle effectively accumulated in the ischemic hindlimb by 24 h post-injection. At Days 10 and 17 post-surgery, the pharmacokinetic profile of ^{64}Cu-RGO-IONP-PEG was significantly different between the naïve and re-injected mice, with the naïve group showing prolonged blood pool uptake while the nanoparticles was rapidly cleared from the circulation of re-injected mice. Also, ischemic hindlimb uptake of ^{64}Cu-RGO-IONP-PEG was lower in re-injected mice (Figure 2).

Quantitative analysis using region of interest (ROI) on organs was used to quantify the PET imaging data. In the naïve group, high %ID/g in blood pool validated the long circulation half-life of RGO-IONP-PEG. Also, nanoparticle localization in the ischemic hindlimb was significantly higher than that of non-ischemic hindlimb at all time points. The highest uptake of nanoparticles in the ischemic hindlimb was found at Day 3 post-surgery (13.3 ± 1.9 %ID/g; n=4), which slowly diminished by Day 10 (11.1 ± 0.8 %ID/g; n=4) and Day 17 post-surgery (2.3 ± 0.3 %ID/g; n=4). From these data, we concluded the capability of effective passive targeting of the nanoparticle (Figure 3a, b). The re-injected group showed lower nanoparticle accumulation in blood pool and higher accumulation in the liver than the naïve group. Also, there was no statistically significance difference the localization of nanoparticles between the non-ischemic and ischemic hindlimb in re-injected mice at Day 10 or Day 17 post-surgery (Figure 3c). Quantitative data of ^{64}Cu-RGO-IONP-PEG accumulation to the organs were determined (Tables S1-3).

Further quantitative analysis was performed using the %ID/g values of each organ. Activity in the blood pool activities was significantly higher in the naïve group at Day 10 and 17 post-surgery in comparison to the re-injected group. Nanoparticle clearance from the blood pool was faster in re-injected mice than naïve mice with circulation half-lives of 22.9 h (naïve group) and 2.0 h (re-injected group) at Day 10 post-surgery, and 35.6 h (naïve group) and 2.3 h (re-injected group) at Day 17 post-surgery (Figure 4a). At 72 h post-injection of nanoparticles, the liver uptake of nanoparticles in the re-injected group was significantly higher than that of the naïve group at Day 10 (40.4 ± 1.2 vs. 26.4 ± 4.2 %ID/g; n=4) and Day 17 (33.4 ± 3.2 vs. 27.3 ± 1.6 %ID/g; n=4), post-surgery (Figure 4b). Meanwhile, nanoparticle accumulation in the ischemic hindlimb was significantly lower in re-injected group than the naïve group with values of 2.3 ± 0.3 vs. 11.1 ± 0.8 %ID/g at Day 10, and 1.8 ± 0.3 vs. 5.2 ± 0.6 %ID/g at Day 17, respectively (n=4; Figure 4c).

Multiple factors can affect the magnitude of ABC phenomenon, with the prominent factor being the time interval between the injection and re-injection of PEGylated materials. Previously, the ABC effect was shown to be most prominent when PEGylated nanomaterials were injected and re-injected in rats within seven days.[16] While this study utilized mice instead of rats, the seven day interval was still employed. Also, the structure and chemical composition of the nanocarriers may impact the magnitude of the ABC effect.[17, 27] It was also shown that the ABC phenomenon occurs with cross-administration of different nanocarriers, and the degree of the ABC effect varied between different nanoparticle combinations.[27] However, there has been no study using inorganic or organic-inorganic hybrid nanoparticles to investigate the ABC phenomenon. In this study, PET imaging and

quantitative analysis clearly verified that the ABC phenomenon was induced by re-injection of the PEGylated organic-inorganic hybrid nanoparticles (i.e. RGO-IONP-PEG).

Ex vivo Biodistribution Study

Ex vivo biodistribution was used to validate the finding of quantitative PET analysis. At Day 10 post-surgery, nanoparticle accumulation in the liver of the re-injected group was significantly higher than the naïve group. In contrast, uptake of the nanoparticle in the other organs of the naïve group was higher than those of the re-injected group, including the blood pool and ischemic hindlimb. The long circulation half-life of RGO-IONP-PEG in the naïve group could attribute to the higher passive targeting of nanoparticles to ischemic hindlimb and non-specific uptakes in the other organs. There was no significant difference between the biodistribution values of the stomach, intestine, skin, and brain (Figure 5a). At Day 17 post-surgery, liver uptake was significantly higher in the re-injected group, while the naïve group displayed nanoparticle localization in circulation, ischemic hindlimb, bone, and lungs (Figure 5b).

Anti-PEG IgM ELISA

Anti-PEG IgM is the most well-known mediator of ABC phenomenon.[28] We measured anti-PEG IgM before injection, and at 7 and 14 days post-injection of ^{64}Cu-RGO-IONP-PEG. Anti-PEG IgM was detectable in the serum of mice at day 7 and 14 post-injection (Figure 6). Hence, the ABC phenomenon in the present study was also likely to be mediated by anti-PEG IgM, similar to the ABC effect elicited by other types of nanomaterials.

Photoacoustic (PA) Imaging

PA imaging was performed to confirm the accumulation RGO-IONP-PEG in the liver by detecting the intrinsic PA imaging properties of RGO. At 72 h post-injection of nanoparticle, the naïve and re-injected mice both showed positive PA signal the liver; yet the signal was much higher in the re-injected mice (Figure 7).

Histological Analysis

Histological examination tissue sections from the naïve and re-injected groups were used to further evaluate nanoparticle accumulation. H&E staining revealed that the nanoparticles accumulated in the Kupffer cells and other phagocytic cells of the liver in both naïve and re-injected groups, yet this accumulation was much higher in the re-injected group. Prussian blue (PB) is used to detect the presence of iron in tissues by the formation of $Fe_4(Fe[CN]_6)_3$, which produces a bright cyan color.[29] Using the PB stain for detecting IONPs, we found enhanced signal in the liver of the re-injected group, while the naïve group showed little IONP accumulation (Figure 8). From these findings, it can be deduced that that the ABC phenomenon increases the amount of nanoparticles sequestered by the liver.

The most compelling mechanism of ABC phenomenon is the anti-PEG immunoglobulin M (IgM) and complement activation-mediated clearance of PEGylated nanomaterials.[16] Specifically, the immune system produces anti-PEG IgM in response to an injection of exogenous PEGylated nanomaterials. When an animal is re-exposed to the PEGylated materials, the re-injected nanomaterials are quickly recognized by the anti-PEG IgM. In

return, this process results in complement activation and removal of the nanomaterials by the mononuclear phagocytic system (MPS). In the present study, we found a positive correlation between anti-PEG IgM and increased liver accumulation of nanoparticles, which resulted from the ABC effect.

ABC phenomenon has been reported in multiple studies using lipid based or polymeric nanocarriers. In the previous studies, the nanocarriers were labeled with radioisotopes or small molecules, because they do not have their own signal. Dam *et al.* used N-Hydroxysuccinimidyl hydrazino nicotinate hydrochloride – distearoyl phosphatidylethanolamine (HYNIC-DSPE) as a chelator for radiolabeling of liposomes.[30] In addition, Ishida *et al.* labeled liposomes with ^{3}H-Cholesterylhexadecyl ether (^{3}H-CHE).[14] Alternatively, Wang *et al.* employed tocopheryl nicotinate (TN) as an indicator by including TN during the formation of lipid based nanocarriers.[27] Therefore, it was challenging to conclude whether the whole nanocarriers or just a labeled subunit was affected by ABC phenomenon. In the present study, we confirmed that the ABC phenomenon induced hepatic clearance of the nanoparticle, which was validated by PA signal from RGO and iron content from IONP. Furthermore, there is no accurate way to confirm the existence of lipid-based or polymeric nanoparticles in the tissue; hence, to the best of our knowledge, the present study is the first report providing histological evidence demonstrating the enhanced accumulation of organic-inorganic hybrid nanoparticles in liver tissue as induced by the ABC phenomenon. While our previous study demonstrated that RGO-IONPs display minimal toxicity in healthy tissues, [20] some studies have shown that RGO may induce intracellular reactive oxygen species.[31] Despite its preclinical use for drug delivery and diagnostic imaging,[32] its low excretability, potential toxicity, and potential interaction with serum proteins have limited the clinical translation of this nanoplatform.

The present study is the first report demonstrating the ABC phenomenon using organic-inorganic hybrid nanoparticles. As multiple types of hybrid nanoparticles display excellent theranostic properties that may allow for clinical translation, deeper insight into the ABC phenomenon is essential for advancing these nanoplatforms to the clinic. In particular, IONP/polymer nanoparticle exhibit a great potential for temperature-responsive drug delivery in various disease models.[33] Also, hybrid quantum dot-liposome nanoparticles have shown minimal toxicity and excellent tumor uptake in cancer models.[34] Hence, the observation of ABC phenomenon with RGO-IONP-PEG may provide valuable insight into the development and clinical translation of other hybrid nanoparticles.

Conclusions

This study further confirms that the ABC phenomenon occurs after re-injection of PEGylated nanoparticles, including ^{64}Cu-RGO-IONP-PEG. This is the first report showing that PEGylated organic-inorganic hybrid nanoparticles can elicit the ABC phenomenon in mice. This process can effectively limit the passive targeting capabilities of nanomaterials to accumulate in ischemic tissues, such as peripheral arterial disease, which was assessed using a murine model of hindlimb ischemia. Furthermore we could show that the nanoparticles were cleared to the liver due to the phenomenon. This observation may be valuable

information which should be considered during developing targeted imaging and/or drug delivery probes using the long circulating PEGylated nanoparticles.

Supplementary Material

Refer to Web version on PubMed Central for supplementary material.

Acknowledgments

This work was supported, in part, by the University of Wisconsin - Madison, the National Institutes of Health (NIBIB/NCI 1R01CA169365, 1R01EB021336, P30CA014520, T32GM08349, T32CA009206, and S10-OD018505), the National Science Foundation (DGE-1256259), and the American Cancer Society (125246-RSG-13-099-01-CCE).

References

1. American Diabetes A. Peripheral Arterial Disease in People with Diabetes. Diabetes Care. 2003; 26:3333–3341. [PubMed: 14633825]
2. Criqui MH, Aboyans V. Epidemiology of Peripheral Artery Disease. Circ Res. 2015; 116:1509–1526. [PubMed: 25908725]
3. Samolsky Dekel BG, Melotti RM, Gargiulo M, Freyrie A, Stella A, Di Nino G. Pain Management in Peripheral Arterial Obstructive Disease: Oral Slow-Release Oxycodone Versus Epidural L-Bupivacaine. Eur J Vasc Endovasc Surg. 2010; 39:774–778. [PubMed: 20335056]
4. Varu VN, Hogg ME, Kibbe MR. Critical Limb Ischemia. J Vasc Surg. 2010; 51:230–241. [PubMed: 20117502]
5. Berger JS, Hiatt WR. Medical Therapy in Peripheral Artery Disease. Circulation. 2012; 126:491–500. [PubMed: 22825411]
6. Dormandy J, Heeck L, Vig S. The Fate of Patients with Critical Leg Ischemia. Semin Vasc Surg. 1999; 12:142–147. [PubMed: 10777241]
7. Tongers J, Roncalli JG, Losordo DW. Therapeutic Angiogenesis for Critical Limb Ischemia: Microvascular Therapies Coming of Age. Circulation. 2008; 118:9–16. [PubMed: 18591450]
8. Amsden BG. Delivery Approaches for Angiogenic Growth Factors in the Treatment of Ischemic Conditions. Expert Opin Drug Deliv. 2011; 8:873–890. [PubMed: 21644842]
9. Violi F, Basili S, Berger JS, Hiatt WR. Antiplatelet Therapy in Peripheral Artery Disease. Handb Exp Pharmacol. 2012:547–563. [PubMed: 22918746]
10. Tu C, Das S, Baker AB, Zoldan J, Suggs LJ. Nanoscale Strategies: Treatment for Peripheral Vascular Disease and Critical Limb Ischemia. ACS Nano. 2015; 9:3436–3452. [PubMed: 25844518]
11. Xu C, Shi S, Feng L, Chen F, Graves SA, Ehlerding EB, Goel S, Sun H, England CG, Nickles RJ, Liu Z, Wang T, Cai W. Long Circulating Reduced Graphene Oxide-Iron Oxide Nanoparticles for Efficient Tumor Targeting and Multimodality Imaging. Nanoscale. 2016
12. Yang K, Feng L, Hong H, Cai W, Liu Z. Preparation and Functionalization of Graphene Nanocomposites for Biomedical Applications. Nat Protoc. 2013; 8:2392–2403. [PubMed: 24202553]
13. Ishida T, Kiwada H. Accelerated Blood Clearance (ABC) Phenomenon Upon Repeated Injection of Pegylated Liposomes. Int J Pharm. 2008; 354:56–62. [PubMed: 18083313]
14. Ishida T, Harada M, Wang XY, Ichihara M, Irimura K, Kiwada H. Accelerated Blood Clearance of Pegylated Liposomes Following Preceding Liposome Injection: Effects of Lipid Dose and Peg Surface-Density and Chain Length of the First-Dose Liposomes. J Control Release. 2005; 105:305–317. [PubMed: 15908032]
15. Koide H, Asai T, Hatanaka K, Urakami T, Ishii T, Kenjo E, Nishihara M, Yokoyama M, Ishida T, Kiwada H, Oku N. Particle Size-Dependent Triggering of Accelerated Blood Clearance Phenomenon. Int J Pharm. 2008; 362:197–200. [PubMed: 18586076]

16. Saadati R, Dadashzadeh S, Abbasian Z, Soleimanjahi H. Accelerated Blood Clearance of Pegylated PLGA Nanoparticles Following Repeated Injections: Effects of Polymer Dose, Peg Coating, and Encapsulated Anticancer Drug. Pharm Res. 2013; 30:985–995. [PubMed: 23184228]
17. Abu Lila AS, Kiwada H, Ishida T. The Accelerated Blood Clearance (ABC) Phenomenon: Clinical Challenge and Approaches to Manage. J Control Release. 2013; 172:38–47. [PubMed: 23933235]
18. Jokerst JV, Lobovkina T, Zare RN, Gambhir SS. Nanoparticle Pegylation for Imaging and Therapy. Nanomedicine (Lond). 2011; 6:715–728. [PubMed: 21718180]
19. England CG, Im HJ, Feng L, Chen F, Graves SA, Hernandez R, Orbay H, Xu C, Cho SY, Nickles RJ, Liu Z, Lee DS, Cai W. Re-assessing the Enhanced Permeability and Retention Effect in Peripheral Arterial Disease Using Radiolabeled Long Circulating Nanoparticles. Biomaterials. 2016; 100:101–109. [PubMed: 27254470]
20. Yang K, Hu L, Ma X, Ye S, Cheng L, Shi X, Li C, Li Y, Liu Z. Multimodal Imaging Guided Photothermal Therapy Using Functionalized Graphene Nanosheets Anchored with Magnetic Nanoparticles. Adv Mater. 2012; 24:1868–1872. [PubMed: 22378564]
21. Orbay H, Hong H, Zhang Y, Cai W. PET/SPECT Imaging of Hindlimb Ischemia: Focusing on Angiogenesis and Blood Flow. Angiogenesis. 2013; 16:279–287. [PubMed: 23117521]
22. Shi S, Orbay H, Yang Y, Graves SA, Nayak TR, Hong H, Hernandez R, Luo H, Goel S, Theuer CP, Nickles RJ, Cai W. PET Imaging of Abdominal Aortic Aneurysm with ^{64}Cu-Labeled Anti-CD105 Antibody Fab Fragment. J Nucl Med. 2015; 56:927–932. [PubMed: 25883125]
23. Yang Y, Hernandez R, Rao J, Yin L, Qu Y, Wu J, England CG, Graves SA, Lewis CM, Wang P, Meyerand ME, Nickles RJ, Bian XW, Cai W. Targeting CD146 with a ^{64}Cu-labeled Antibody Enables in Vivo Immunopet Imaging of High-Grade Gliomas. Proc Natl Acad Sci U S A. 2015; 112:E6525–6534. [PubMed: 26553993]
24. Yang XY, Zhang XY, Ma YF, Huang Y, Wang YS, Chen YS. Superparamagnetic Graphene Oxide-Fe3O4 Nanoparticles Hybrid for Controlled Targeted Drug Carriers. J Mater Chem. 2009; 19:2710–2714.
25. Slovut DP, Lipsitz EC. Surgical Technique and Peripheral Artery Disease. Circulation. 2012; 126:1127–1138. [PubMed: 22927475]
26. Kim J, Cao L, Shvartsman D, Silva EA, Mooney DJ. Targeted Delivery of Nanoparticles to Ischemic Muscle for Imaging and Therapeutic Angiogenesis. Nano Lett. 2011; 11:694–700. [PubMed: 21192718]
27. Wang C, Cheng X, Su Y, Pei Y, Song Y, Jiao J, Huang Z, Ma Y, Dong Y, Yao Y, Fan J, Ta H, Liu X, Xu H, Deng Y. Accelerated Blood Clearance Phenomenon Upon Cross-Administration of Pegylated Nanocarriers in Beagle Dogs. Int J Nanomedicine. 2015; 10:3533–3545. [PubMed: 25999716]
28. Hashimoto Y, Shimizu T, Abu Lila AS, Ishida T, Kiwada H. Relationship between the Concentration of Anti-Polyethylene Glycol (PEG) Immunoglobulin M (IgM) and the Intensity of the Accelerated Blood Clearance (ABC) Phenomenon against Pegylated Liposomes in Mice. Biol Pharm Bull. 2015; 38:417–424. [PubMed: 25757923]
29. Schlorf T, Meincke M, Kossel E, Gluer CC, Jansen O, Mentlein R. Biological Properties of Iron Oxide Nanoparticles for Cellular and Molecular Magnetic Resonance Imaging. Int J Mol Sci. 2010; 12:12–23. [PubMed: 21339973]
30. Dams ET, Laverman P, Oyen WJ, Storm G, Scherphof GL, van Der Meer JW, Corstens FH, Boerman OC. Accelerated Blood Clearance and Altered Biodistribution of Repeated Injections of Sterically Stabilized Liposomes. J Pharmacol Exp Ther. 2000; 292:1071–1079. [PubMed: 10688625]
31. Dutta T, Sarkar R, Pakhira B, Ghosh S, Sarkar R, Barui A, Sarkar S. Ros Generation by Reduced Graphene Oxide (RGO) Induced by Visible Light Showing Antibacterial Activity: Comparison with Graphene Oxide (GO). RSC Advances. 2015; 5:80192–80195.
32. Yang K, Feng L, Hong H, Cai W, Liu Z. Preparation and Functionalization of Graphene Nanocomposites for Biomedical Applications. Nat Protoc. 2013; 8:2392–2403. [PubMed: 24202553]
33. Vivero-Escoto JL, Huang YT. Inorganic-Organic Hybrid Nanomaterials for Therapeutic and Diagnostic Imaging Applications. Int J Mol Sci. 2011; 12:3888–3927. [PubMed: 21747714]

34. Al-Jamal WT, Al-Jamal KT, Bomans PH, Frederik PM, Kostarelos K. Functionalized-Quantum-Dot-Liposome Hybrids as Multimodal Nanoparticles for Cancer. Small. 2008; 4:1406–1415. [PubMed: 18711753]

Abbreviations

PAD	peripheral arterial disease
ABC	accelerated blood clearance
PEG	polyethylene glycol
CLI	critical limb ischemia
AFM	atomic force microscopy
IONP	iron oxide nanoparticles
MRI	magnetic resonance imaging
PET	positron emission tomography
RGO	reduced graphene oxide
%ID/g	percent injected dose per gram of tissue

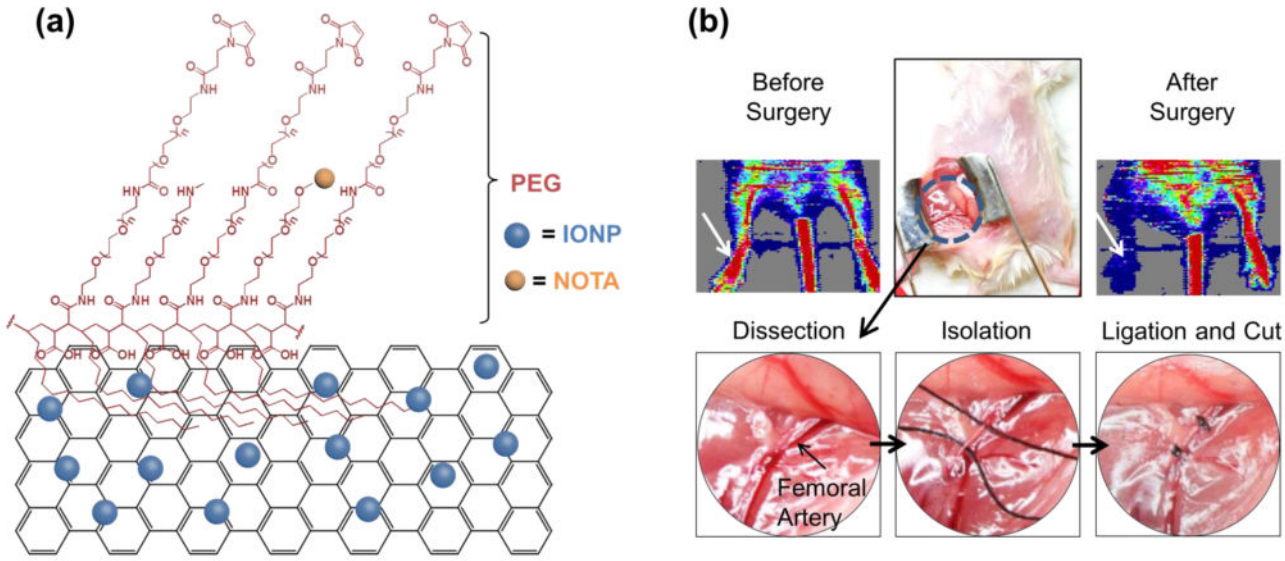

Figure 1.

PEGylated reduced graphene oxide – iron oxide nanoparticles (RGO-IONP-PEG) for imaging of peripheral arterial disease in a mouse model of hindlimb ischemia. (a) Schematic drawing of RGO-IONP-PEG nanoparticle. On a sheet of reduced graphene oxide (RGO), iron oxide nanoparticles (IONPs) are conjugated (RGO-IONP). RGO-IONP was functionalized with NOTA and two layers of PEG. (b) The murine model of hindlimb ischemia is a representative model of human PAD. A mid-abdominal incision was made and the adjacent fat tissue and fascia were dissected to visualize the femoral artery for isolation, ligation, and cutting to produce the ischemic hindlimb. White arrow indicates the surgical hindlimb in the Doppler ultrasound imaging. Doppler ultrasound imaging revealed significantly decreased red signal in the ischemic hindlimb, indicating decreased blood flow and confirming the successful generation of the PAD model.

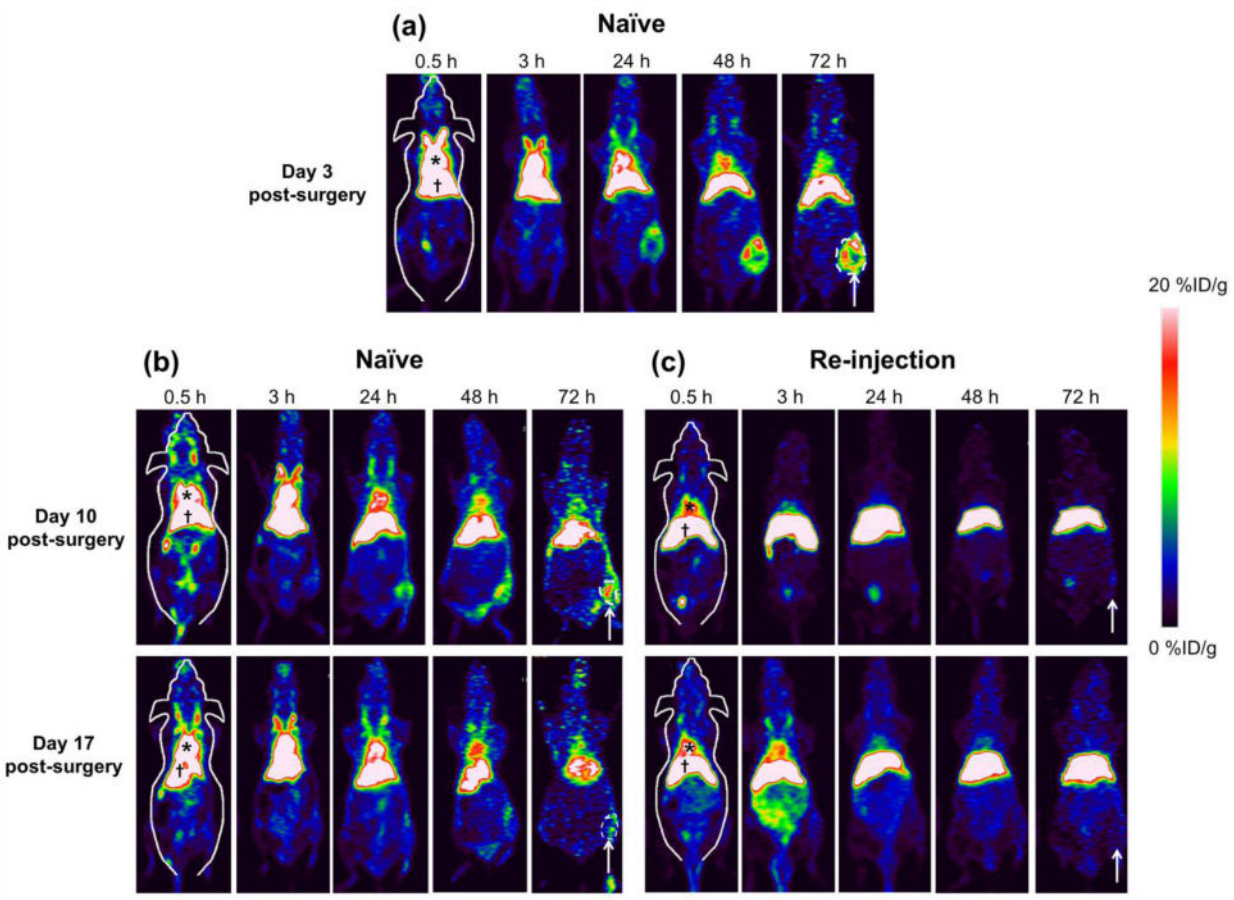

Figure 2.

PET imaging of ^{64}Cu-RGO-IONP-PEG in mice. PET imaging was performed at 3, 10, and 17 days post-surgical induction of hindlimb ischemia in mice. Images were acquired from 30 min to 72 h after nanoparticle injection. (a) At Day 3 post-surgery, high nanoparticle accumulation in circulation and the ischemic hindlimb was found. (b, c) At Day 10 and 17 post-surgery, the naïve group showed prolonged blood pool uptake, yet the re-injected group showed significantly lower uptake in the blood pool. Nanoparticle uptake in the ischemic hindlimb of re-injected mice was lower than that of naïve group at Day 10 and 17 post-surgery. The region of interest used for quantitative analysis is outlined in white for the naïve group. * = blood pool, † = liver, white arrow = ischemic hindlimb.

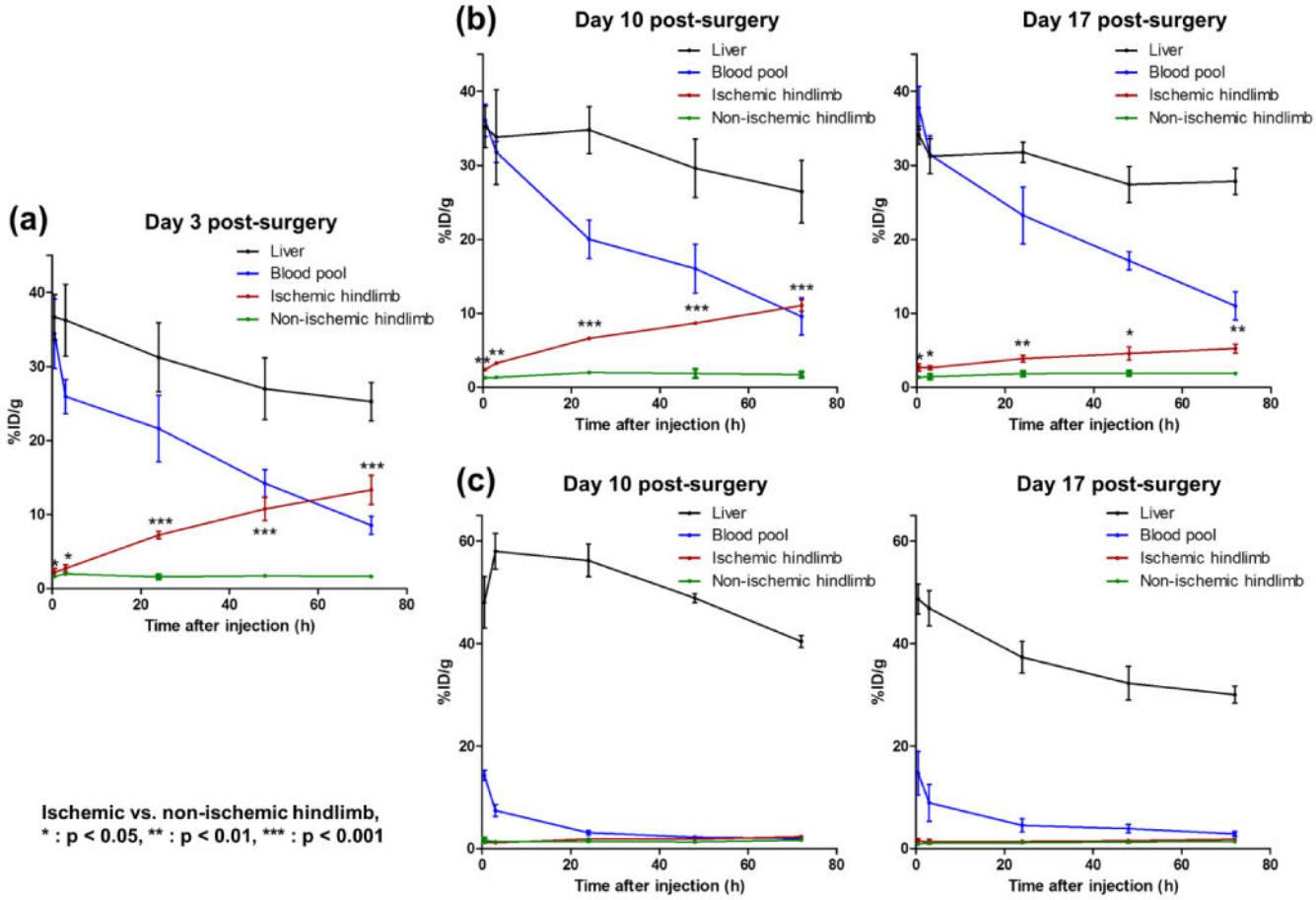

Figure 3.

Pharmacokinetics of ^{64}Cu-RGO-IONP-PEG in hindlimb ischemia-induced mice (a) At Day 3 post-surgery, the nanoparticle displayed excellent stability in the blood pool, with significantly higher uptake in ischemic hindlimb than the non-ischemic hindlimb. (b) The long circulation half-life of ^{64}Cu-RGO-IONP-PEG was found in the naïve group at Day 10 and 17 post-surgery. Also, nanoparticle accumulation in the ischemic hindlimb remained significantly higher than that of non-ischemic hindlimb, although the values were lower than Day 3 post-surgery. (c) Decreased circulation half-life and increased liver sequestration was found in the re-injected group. Nanoparticle localization in the ischemic hindlimb was similar to that of the non-ischemic hindlimb. Each value represents the mean ± SD (n=4).

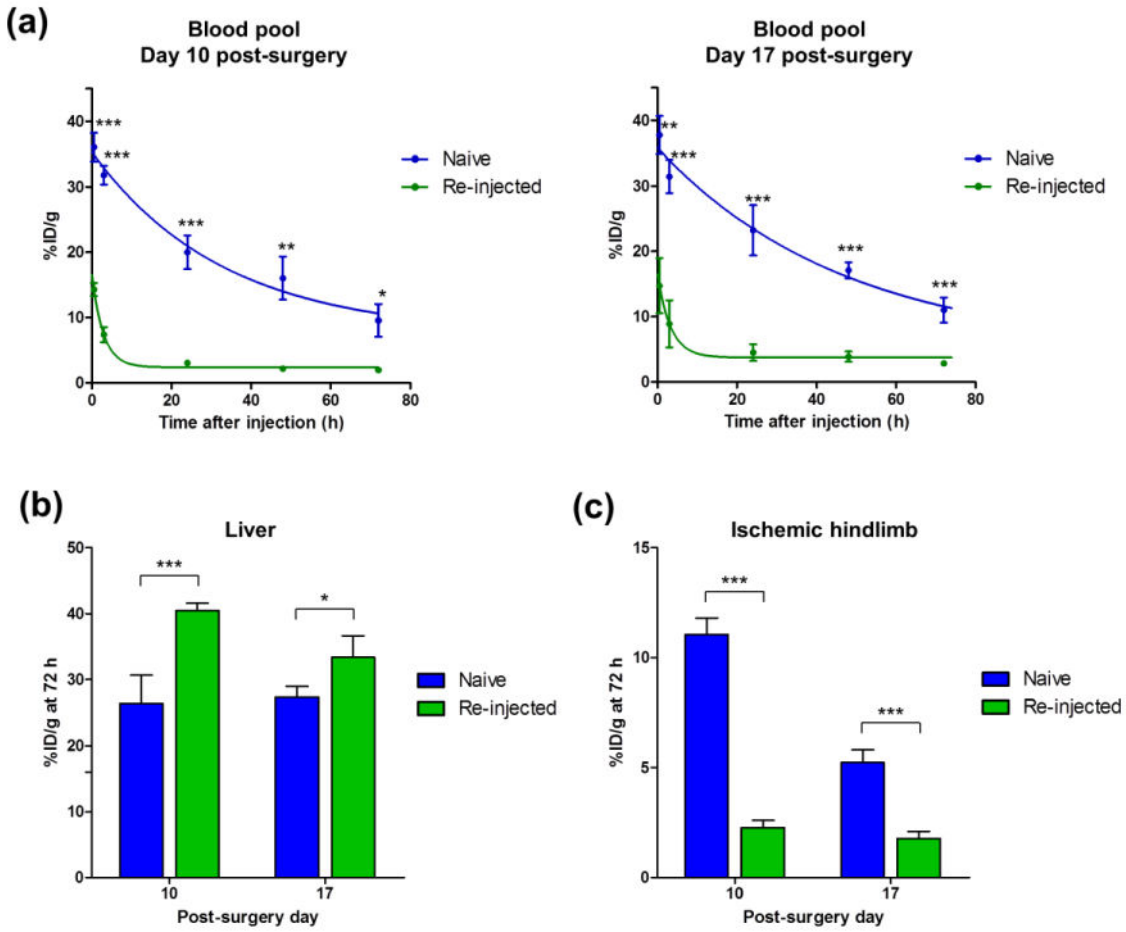

Figure 4.

Comparison of nanoparticle pharmacokinetics in the blood pool, liver, and ischemic hindlimb between naïve and re-injected mice. (a) Blood pool activity in the naïve group was consistently higher than that of the re-injected group. (b) Liver uptake of nanoparticle at 72 h after injection was compared between the naïve and re-injected group. Liver uptake was higher in the re-injected group than the naïve group at Day 10 and 17 post-surgery. (c) Nanoparticle uptake in the ischemic hindlimb at 72 h post-injection was higher in the naïve group than the re-injected group at Day 10 and 17. Each value represents the mean ± SD (n=4). Naïve vs. Re-injected, * : $p < 0.05$, ** : $p < 0.01$, *** : $p < 0.001$.

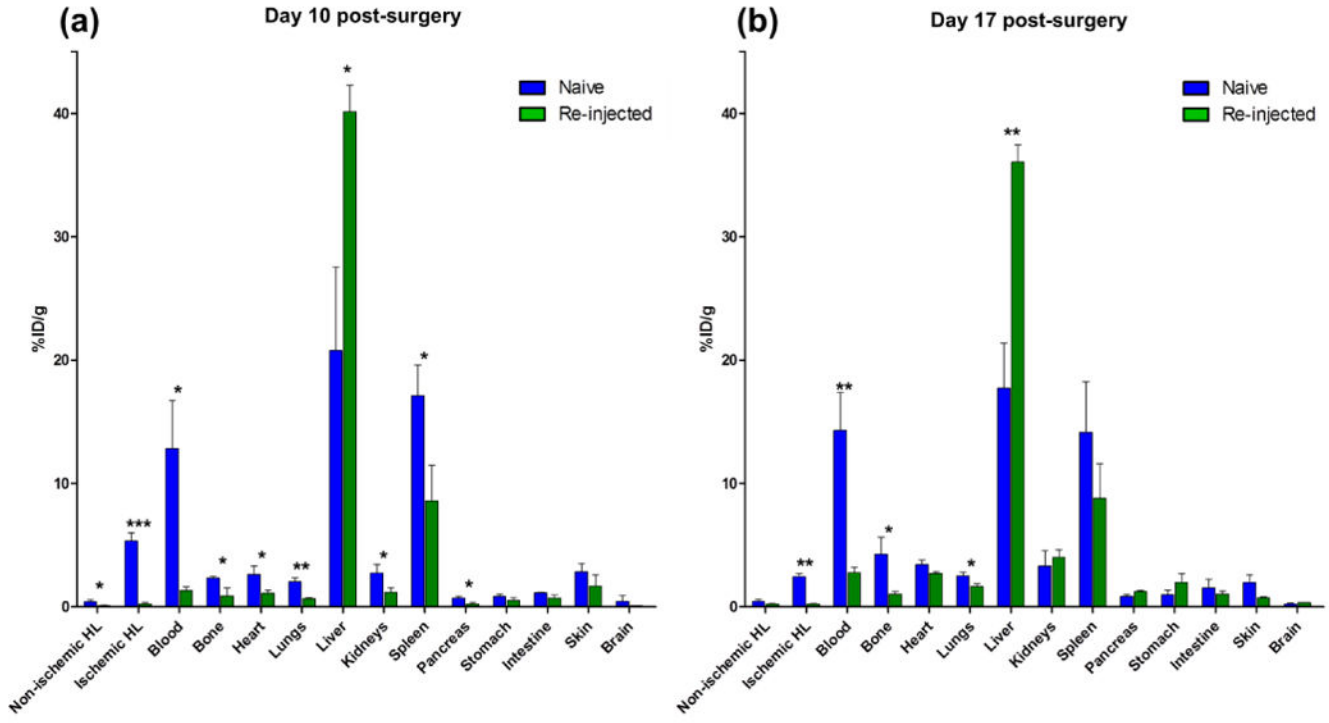

Figure 5.

Comparison of ex vivo biodistribution between the naïve and re-injected group at (a) Day 10 and (b) Day 17. Each value represents the mean ± SD (n=4). HL: hindlimb, Naïve vs. Re-injected, * : $p < 0.05$, ** : $p < 0.01$, *** : $p < 0.001$

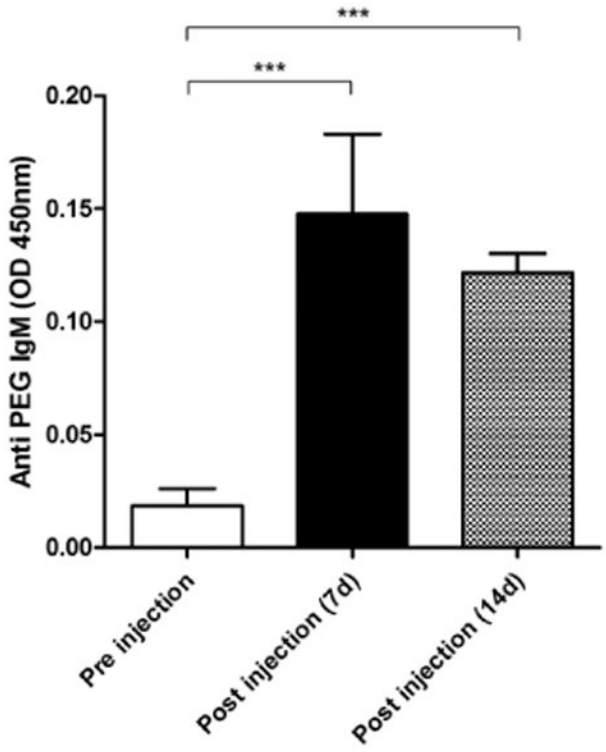

Figure 6.

ELISA for anti-PEG IgM antibody. At 7 and 14 days after injection of ^{64}Cu-RGO-IONP-PEG, the presence of anti-PET IgM was detected in mouse serum by ELISA. Each value represents the mean ± SD (n=4).

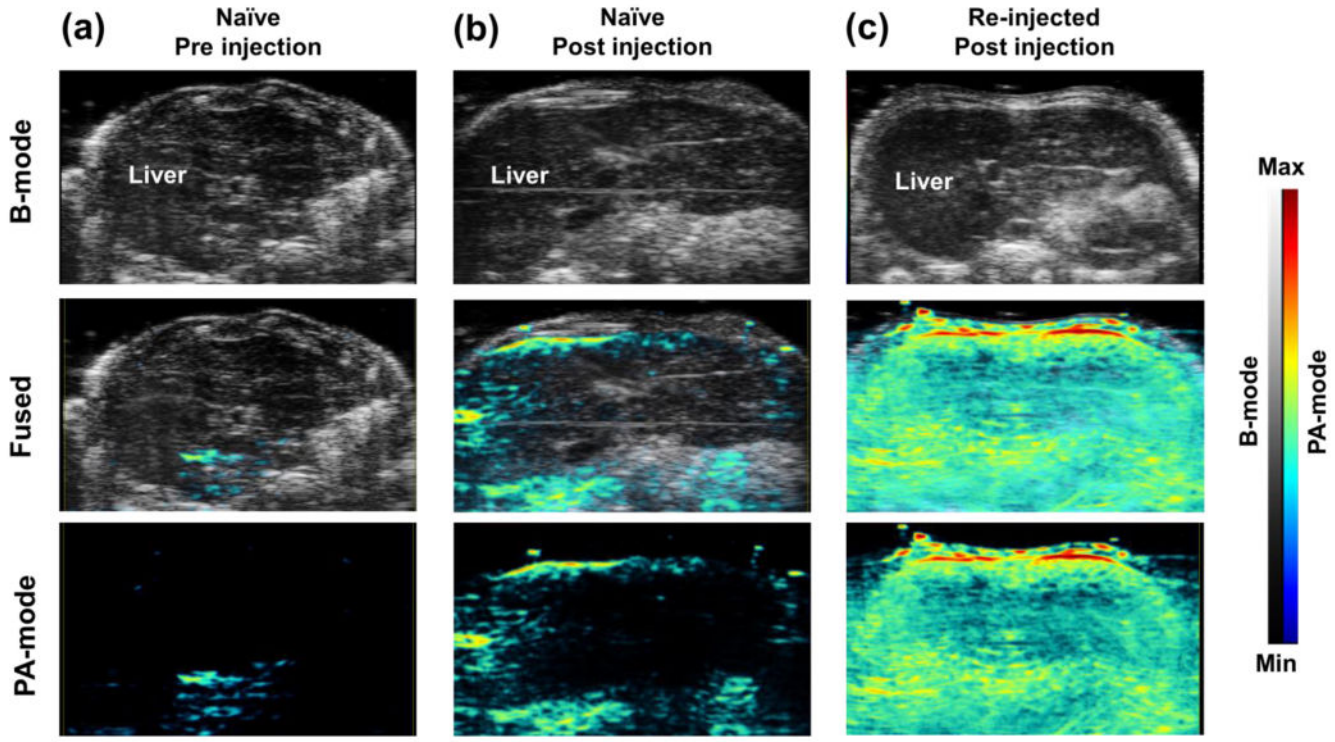

Figure 7.

Photoacoustic imaging confirms the liver uptake of RGO-IONP-PEG. Ultrasound imaging (B-mode), which was utilized for anatomical information and photoacoustic imaging (PA-mode) were obtained simultaneously. Increased PA signal validated the existence of nanoparticles in the liver. (a) PA signal was low in the naïve group before injection. (b, c) The PA signal was enhanced in both naïve and re-injected mice at 72 h post-injection of the nanoparticles. The re-injected group showed higher PA signal in the liver than the naïve group. B-mode: Brightness mode, PA-mode: Photoacoustic mode

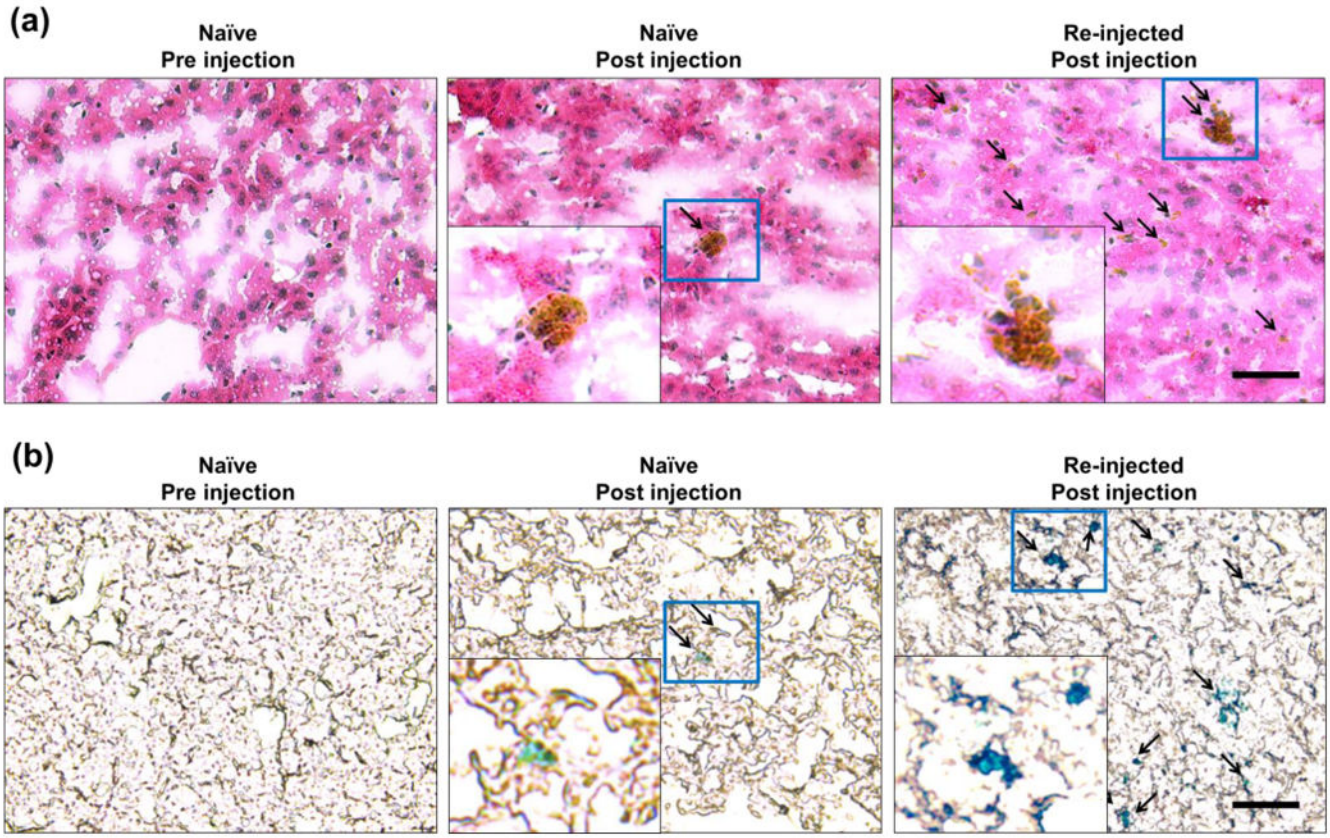

Figure 8.

H&E and Prussian blue (PB) staining of liver tissue sections. (a) H&E staining of the liver tissues revealed no cells with nanoparticles accumulation from pre-injected naïve group. Minimal nanoparticle presence was found in the liver sections from the naïve group after receiving an injection of nanoparticles. Liver sections from the re-injected mice showed high cellular uptake of nanoparticles. Black arrows indicate the presence of nanoparticles within the cell. (b) PB staining validated the findings from H&E, showing no iron contents in pre-injected naïve mice and high nanoparticle accumulation in the naïve group after nanoparticle injection and in re-injected mice.